Crack healing behaviour of Cr_2AlC MAX phase studied by X-ray tomography

Pei, R.; McDonald, S. A.; Shen, L.; van der Zwaag, S.; Sloof, W. G.; Withers, P. J.; Mummery, P. M.

DOI
10.1016/j.jeurceramsoc.2016.07.018

Publication date
2017

Document Version
Final published version

Published in
Journal of the European Ceramic Society

Journal of the European Ceramic Society 37 (2017) 441–450

Contents lists available at www.sciencedirect.com

Journal of the European Ceramic Society

journal homepage: www.elsevier.com/locate/jeurceramsoc

Crack healing behaviour of Cr_2AlC MAX phase studied by X-ray tomography

R. Pei [a], S.A. McDonald [a], L. Shen [b], S. van der Zwaag [c], W.G. Sloof [b], P.J. Withers [a], P.M. Mummery [d,*]

[a] School of Materials, University of Manchester, Manchester M13 9PL, UK
[b] Department of Materials Science and Engineering, Delft University of Technology, Mekelweg 2, 2628 CD Delft, The Netherlands
[c] Novel Aerospace Materials Group, Faculty of Aerospace Engineering, Delft University of Technology, Kluyverweg 1, 2629 HS, Delft, The Netherlands
[d] School of Mechanical, Aerospace and Civil Engineering, University of Manchester, Manchester M13 9PL, UK

ARTICLE INFO

Article history:
Received 30 March 2016
Received in revised form 16 July 2016
Accepted 18 July 2016
Available online 16 September 2016

Keywords:
Cr2AlC
X-ray tomography
Crack healing
Correlative study

ABSTRACT

The autonomous crack-healing capability of Cr_2AlC MAX phase ceramic by surface oxidation at elevated temperatures has a huge potential for high temperature structural and protective coating applications. In this work we use time-lapse X-ray computed tomography (CT) to track the fine details of local crack filling phenomena in 3 dimensions (3D) with time. The maximum crack width that could be fully healed upon exposure to 1200 °C in air is 4.8 μm in 4 h and 10 μm after 12 h. Furthermore, during healing Cr_7C_3 phase is observed beneath the dense Al_2O_3 layer (average thickness of 1 μm on each crack surface) when the crack width exceeds 2 μm. The 3D image sequences indicated that the rate of healing is essentially independent of position along, or across, the crack faces. The crack healing kinetics of Cr_2AlC at 1200 °C broadly follows a parabolic rate law with a rate constant of 4.6×10^{-4} μm^2 s^{-1}. The microstructure, composition and thickness of the oxide scale in the healed crack area are characterized via post mortem SEM-EDS measurements and confirm the formation of an initial dense alumina layer on top of which a more porous layer forms. Impurity Cr particles appear to accelerate the oxidation process locally and correlative SEM imaging of the same region suggests this is by providing Cr_2O_3 nucleation sites.

1. Introduction

Recently, layered ternary ceramic compounds having the composition $M_{n+1}AX_n$ (n = 1, 2 or 3) where M is an early transition metal, A is an element in either the IIIA or IVA group and X is C or N (known collectively as MAX phase ceramics) have attracted a lot of attention [1,2]. These materials exhibit an unusual combination of properties, such as high strength and modulus, excellent oxidation resistance, low density, thermal shock resistance, damage tolerance as well as good machinability [3–8]. Therefore, they are good candidates for high temperature applications, such as gas turbine components, heat exchangers, oxidation resistant coatings, etc. However, being a ceramic, they still bear the common drawbacks of low toughness and sensitivity to surface defects and cracks, which may reduce their reliability.

Recent research showed that these materials exhibit self-healing capability when they are exposed to an oxidizing environment at high temperatures [9–12]. Given their potential applications as high temperature structural materials, such autonomous healing capability would greatly improve their reliability and potentially reduce maintenance costs. Extensive studies have been done on the Ti-Al-C ternary system. Song and co-workers reported that in Ti_3AlC_2 ceramic a crack with average width of 5 μm was healed by a heat treatment at 1100 °C for 2 h in air [13]. Yang and co-workers reported that notches cut by focused ion beam (FIB) of 2 μm width in Ti_2AlC ceramic were healed by a heat treatment at 1200 °C for 1 h in air [9]. The self-healing of Ti-Al-C MAX phase ceramic proceeds by oxidation, whereby cracks, gaps or notches are filled by α-Al_2O_3 and rutile-TiO_2 through oxidation induced volume expansion [14]. Our recent work utilized the synchrotron X-ray tomography to monitor the cracking and healing of Ti_2AlC MAX phase ceramics, showing a decreased mechanical strength recovery in the second healing cycle, due to the formation of a weak and porous TiO_2 phase [15]. Consequently, it would be desirable if

* Corresponding author.
E-mail address: ruizhi.pei@postgrad.manchester.ac.uk (R. Pei).

http://dx.doi.org/10.1016/j.jeurceramsoc.2016.07.018
0955-2219/

the crack gap was filled solely by the strong Al_2O_3 phase providing optimal strength recovery after healing.

Previous research on Cr_2AlC showed that the oxidation product at high temperatures is primarily Al_2O_3 [16–19], potentially offering better recovery of strength after healing than Ti-Al-C MAX phase ceramics. Li studied the strength recovery of Cr_2AlC after healing at 1100 °C in air for 4–100 h and reported that the strength recovery of Cr_2AlC has a strong dependence on healing time, with better strength recovery after increasing healing time [20]. Therefore, understanding the kinetics of healing is critical for predicting the healing strength recovery. Until now, crack healing kinetic studies of Cr_2AlC have relied on thermogravimetric analysis (TGA) experiments performed on planar surfaces and there are still some arguments on its isothermal oxidation behaviour [16,18]. The isothermal oxidation kinetics of Cr_2AlC was first reported by Lin to obey a parabolic law at 1200 °C in air [21]. Tian studied the isothermal behaviour of Cr_2AlC at 1100 and 1250 °C in air for 20 h and confirmed the parabolic relation [16]. While Lee reported that the oxidation curve deviated negatively from a parabolic rate law at temperature above 1100 °C [18]. Recently, Li studied the isothermal oxidation of Cr_2AlC at 1100 and 1200 °C in air for 100 h and reported that the oxidation kinetics of Cr_2AlC followed a cubic law rather than a parabolic one [20].

Besides these inconsistencies, the oxidation kinetics of Cr_2AlC measured by TGA on a polished planar surface could be inaccurate or even misleading when considering the healing of real cracks. The crack healing is an inherently three-dimensional process. Factors such as crack shielding and oxygen transport within the crack should be considered when building a realistic crack-healing model. However, these factors cannot be taken into account from 2D measurements. Therefore, it would be beneficial if the crack healing behaviour of real cracks could be directly followed over time not only in two dimensions (2D) but also in three dimensions (3D). Recently high resolution X-ray CT has been exploited to image and quantify the repair and re-cracking of Ti_2AlC MAX phase ceramic in situ and in 3D over time for the first time using large scale synchrotron X-ray computed tomography (CT) [15]. Here, we use high-resolution laboratory X-ray microtomography to study high temperature self-healing of Cr_2AlC to obtain quantitative information on crack healing kinetics and healing uniformity along and across the crack.

2. Experiment

Bulk Cr_2AlC ceramic was prepared using a mixture of high purity Cr (>99.2%, average particle size of 100 μm), Al (>99.8%average particle size of 45 μm) and graphite (>99.5%, average particle size of 6 μm) powders with a molar ratio of Cr:Al:C = 2:1.15:1. A slight excess of Al was added to compensate for its loss during sintering, cf. [22]. These powders were mixed for 3 h in a tumble mixer using zirconia balls and then cold pressed with a pressure of 300 MPa into tablets with a diameter of 25 mm and a thickness of about 5 mm with a Carver press. Next, the tablets were put into a graphite boat and pressure-less sintered (PLS) in a tube furnace (Lenton Furnaces, PTF 16/75/610) under an argon flow (>5 N) at 1400 °C for 1 h. Subsequently, the PLS sintered samples were pulverized and sintered in a spark plasma sintering furnace (HP D 25, FCT Systeme) at 1250 °C for 1 h in flowing argon under a pressure of 50 MPa, yielding an almost fully dense material (relative density > 99.4%).

The Cr_2AlC specimen for the X-ray microtomography investigation was machined to a 7.5 mm long cylinder of 2.5 mm diameter. A 2.5 mm wide chevron notch of 40° was introduced into the sample by wire electrical discharge machining (EDM) to help to initiate a stable crack. Crack initiation and growth was performed using a mechanical tester (MTS Alliance RT/100) with a 15° wedge made of a Ni-based superalloy and applying a displacement rate of 0.001 mm/min. A tomography scan was taken once the initial crack was clearly visible in the X-ray projections but the sample was still mechanically intact. Subsequently the cracked Cr_2AlC specimen was healed at 1200 °C in a box furnace (Carbolite BWF) over a period of 12 h intermittently, while removing it every 4 h to record an X-ray microtomography scan.

The high resolution X-ray tomography experiment was performed at the Henry Moseley X-ray Imaging Facility, University of Manchester, using a Zeiss Xradia Versa 500. The Cr_2AlC sample was mounted on a rotation stage, between the X-ray source and detector. The X-ray source-sample and the sample-detector distances were 12 mm and 48 mm respectively. The CT data was collected using a detector system consisting of objective lens having ×4 optical magnifications and a 16-bit 2000 × 2000 pixellated detector, giving a field of view of 1.346 × 1.374 mm and an effective voxel size in the reconstructed data of 0.68 × 0.68 × 0.68 μm^3. The accelerating voltage was set to 90 kV to maximize the contrast between Al_2O_3 and the Cr_2AlC matrix. For each scan, a total of 1441 equally spaced projections were collected over 360° with each projection acquired in 45 s. The X-ray tomography reconstructions were computed using a Feldkamp-Davis-Kress (FDK) algorithm. Image processing and analysis was performed using FEI Avizo 8.0 software.

To study the microstructure characteristic of the healing oxide, a second Cr_2AlC sample containing a 1000 μm long, <13 μm wide crack was exposed at 1200 °C in air for 4 h. The sample after heat treatment was ground with SiC paper and finished with colloidal silica. The cross section of the healed area was characterized by Philips XL30 ESEM-FEG and FEI Quanta 650 scanning electron

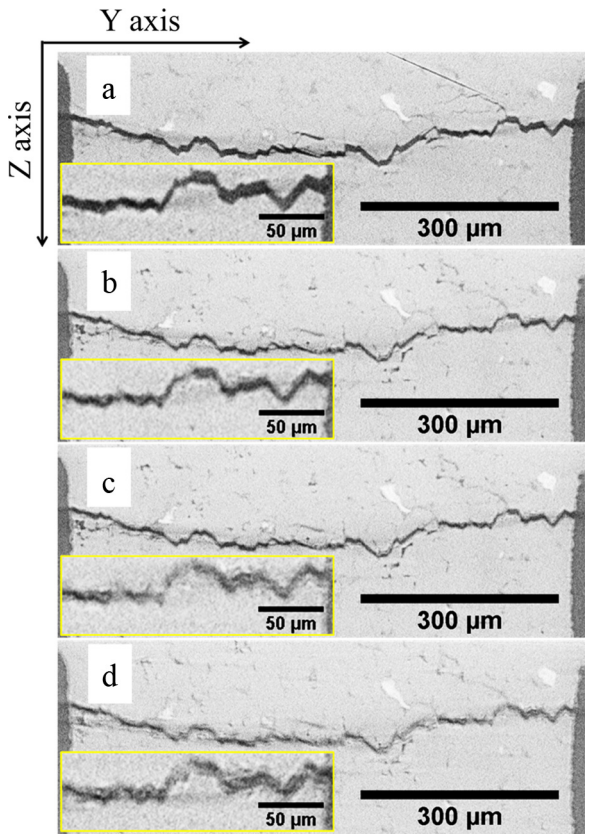

Fig. 1. 2D X-ray tomographic virtual cross-sections through the crack, grown in the X-direction at different stages of healing: (a) as-cracked; (b) after 4 h; (c) after 8 h; and (d) after 12 h exposure to 1200 °C in air. Magnified regions of the crack are shown inset.

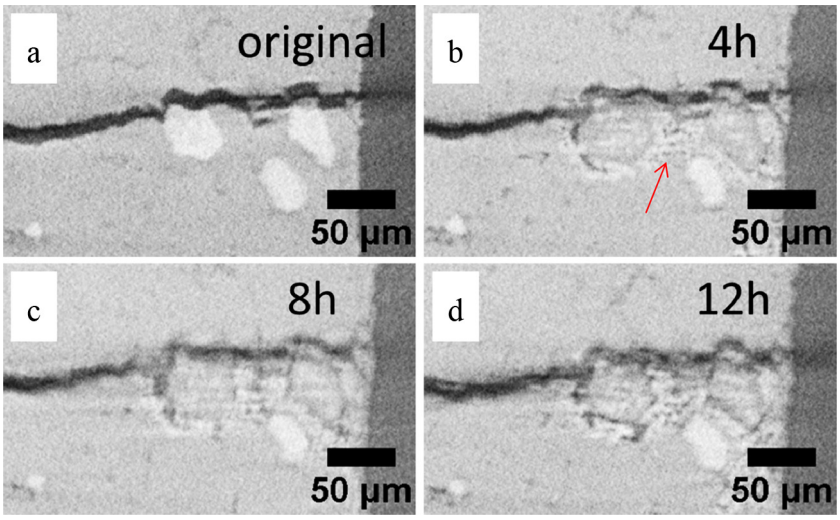

Fig. 2. 2D X-ray tomographic cross sections with surface breaking Cr particles at different healing stages: (a) original; (b) after 4 h healing at 1200 °C in air; (c) after 8 h healing at 1200 °C in air; (d) after 12 h healing at 1200 °C in air.

microscopes equipped with X-ray microanalysis (XMA) systems using energy-dispersive spectrometry (EDS).

3. Results

3.1. 2D X-ray tomographic cross sections of crack at different healing stages

Virtual slices through the X-ray tomographs perpendicular to the crack growth (x) direction are shown in Fig. 1. The light particles having diameters from 10 μm to 30 μm were identified by EDS to be Cr particles and probably were the result of a locally incomplete reaction during the sintering process.

As shown in Fig. 1a the initial crack width (opening) before heat treatment is around 10 μm. It is evident that the gap between the crack faces decreases progressively with thermal exposure time (from Fig. 1a–d). After 12 h heat treatment at 1200 °C in air, some parts of the crack are partially healed as shown in Fig. 1d. Given that previously a crack of similar width in Ti_2AlC was observed to heal at the same temperature in less than one hour [14], it is clear that the healing rate of Cr_2AlC is significantly slower. The contrast within the cracked area is seen to lighten somewhat in certain regions, indicating that parts of the crack have been filled by oxide having an X-ray absorption coefficient higher than air but lower than the Cr_2AlC matrix. The oxide was later confirmed by scanning electron microscopy and EDS to primarily comprise Al_2O_3.

Another interesting phenomenon is that the presence of Cr particles close to the crack surface appears to significantly increase the local healing kinetics, as shown in Fig. 2. It is clear that an oxide layer with a thickness of around 7 μm was formed after 4 h healing on the crack surface adjacent to Cr particles, while the thickness of the oxide layer formed in the remaining areas of the crack surface was around 2 μm. During the healing process, the surface breaking Cr particles that were directly exposed to air have reacted with the environment forming secondary phases as well as some "micro voids" near the original interface with the matrix, as indicated by the red arrow in Fig. 2b. Upon reaction the contrast of the particles darkens, becoming slightly darker than the matrix which suggests a much lower local Cr content. However, the non-surface breaking Cr particles remained unchanged during the healing process as shown in Figs. 1 and 2. This result indicates that the Cr particles are stable upon exposed to heat treatment at 1200 °C. The difference

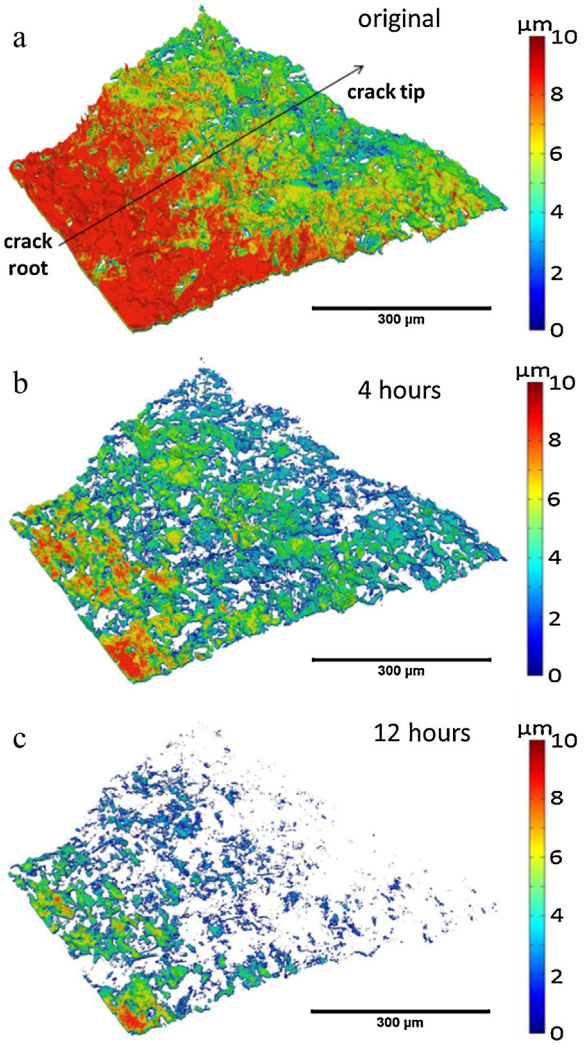

Fig. 3. Three-dimensional CFG maps (measured in microns) calculated for increasing exposure times: (a) as-cracked; (b) after 4 h and (c) after 12 h' healing at 1200 °C in air.

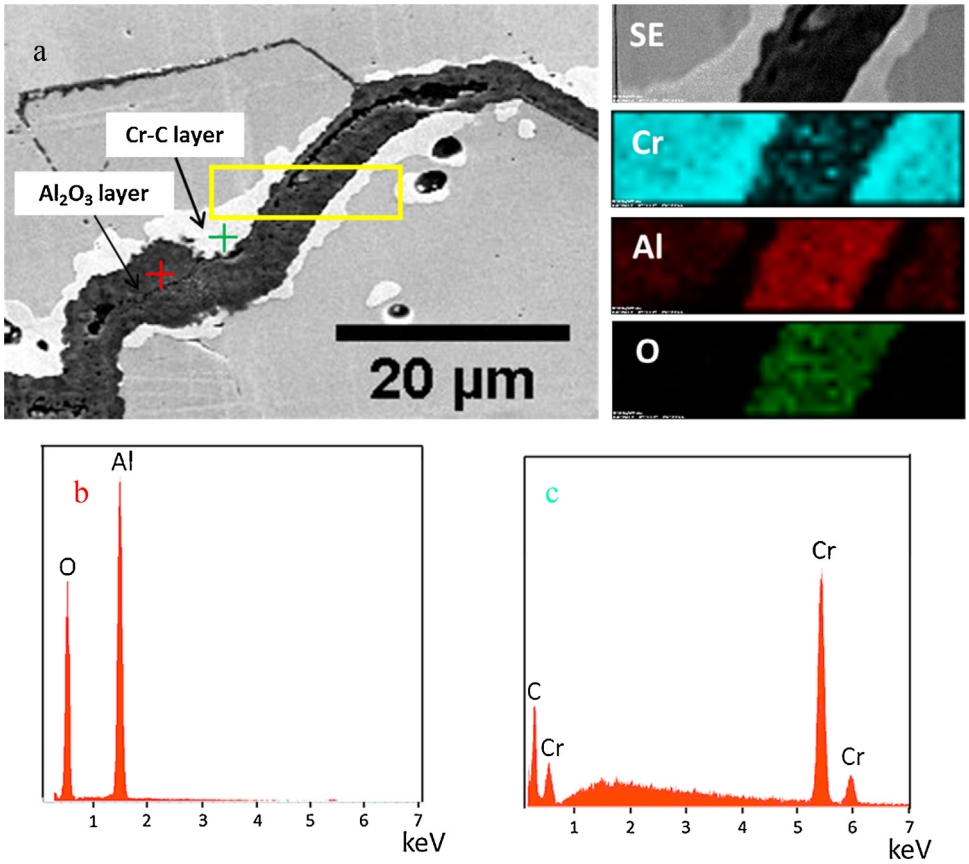

Fig. 4. (a) Secondary electron cross-sectional SEM image and corresponding elemental maps of crack area after healing at 1200 °C in air for 4 h. (b–c) X-ray spectra acquired at the locations indicated by red and green crosses in Fig. 4a respectively.

during the healing process of these two types of Cr particles should be attributed to the direct exposure to air.

3.2. 3D crack face gap maps at different stages of healing

The 3D crack face gap (CFG) has been mapped, and the result is shown in Fig. 3. The 3D crack volume was segmented using greyscale thresholding in FEI Avizo software from which the crack face gap was calculated from the segmented 3D crack volume using Matlab [23]. The 3D CFG map was then generated by covering the 3D crack surface with a colourmap representing the extent of crack face gap. The trapezoid shape of the 3D CFG map is due to the chevron-notch geometry of the sample. Considering the fact that the change in crack face gap between 8 h and 12 h is small, the present work focuses on a detailed description of the CFG map obtained after 12 h.

By comparing the 3D CFG map for the sample in the as-cracked state (Fig. 3a) with that after 4 h thermal treatment (Fig. 3b), it can be seen that the crack width decreases more or less uniformly over the whole crack area during healing. After 12 h of heat treatment, the crack tip area was almost fully healed, as shown in Fig. 3c. It is worth noting that as the exposure time increased, some crack areas became isolated from the environment due to uneven local healing leading to a local slowing of the crack-healing. This could mean that some internal islands remain unhealed even after prolonged exposure. However, in general the region nearest crack tip healed first and the healed zone developed in the opposite direction to that of crack growth as what remained of the crack retreated towards the root.

3.3. Microstructure of healed area

To study the microstructure of the healed area, a second cracked Cr_2AlC sample was healed at 1200 °C in air for 4 h and then sectioned along the crack growth direction. The sectioned surfaces were analysed by SEM and elemental EDS. A typical secondary electron cross-sectional SEM image and the corresponding elemental maps of the healed area are shown in Fig. 4a. The healed area comprises three layers: a central dark layer and two brighter layers on either side. By EDS mapping the dark contrast layer was confirmed to be primarily Al_2O_3, while the two bright layers were confirmed to be Cr_7C_3; see Fig. 4b and c. This result is consistent with previous oxidation experiment conducted by Lee [18], Tian [16], and Li [24], where an outer layer of primarily Al_2O_3 and a sublayer of Cr_7C_3 were observed at the same temperature. Unlike Ti_2AlC, where porous TiO_2 phase is usually found in healed regions [11], no Cr_2O_3 layer was detected in the healed area of Cr_2AlC.

The microstructures of the healed area in four different positions b1, b2, b3 and b4 (indicated by the yellow rectangles) from crack root to crack tip are shown in Fig. 5. It can be seen in Fig. 5 (b1 and b2) that after 4 h annealing at 1200 °C in air, the crack was not fully healed near the crack root. However, the crack was almost fully healed at b3 and b4. The average thickness of Al_2O_3 on a single crack surface is comparable in positions b1, b2 and b3, indicating a similar healing rate all along the crack, as quantified in Table 1. Given that the Al_2O_3 formed on both crack surfaces, the maximum crack width that could be healed by Al_2O_3 formation at 1200 °C in 4 h is estimated to be around 4.8 μm.

It is worth noting that the crack in position b4 was healed purely by Al_2O_3 and no Cr_7C_3 was observed. The absence of Cr_7C_3

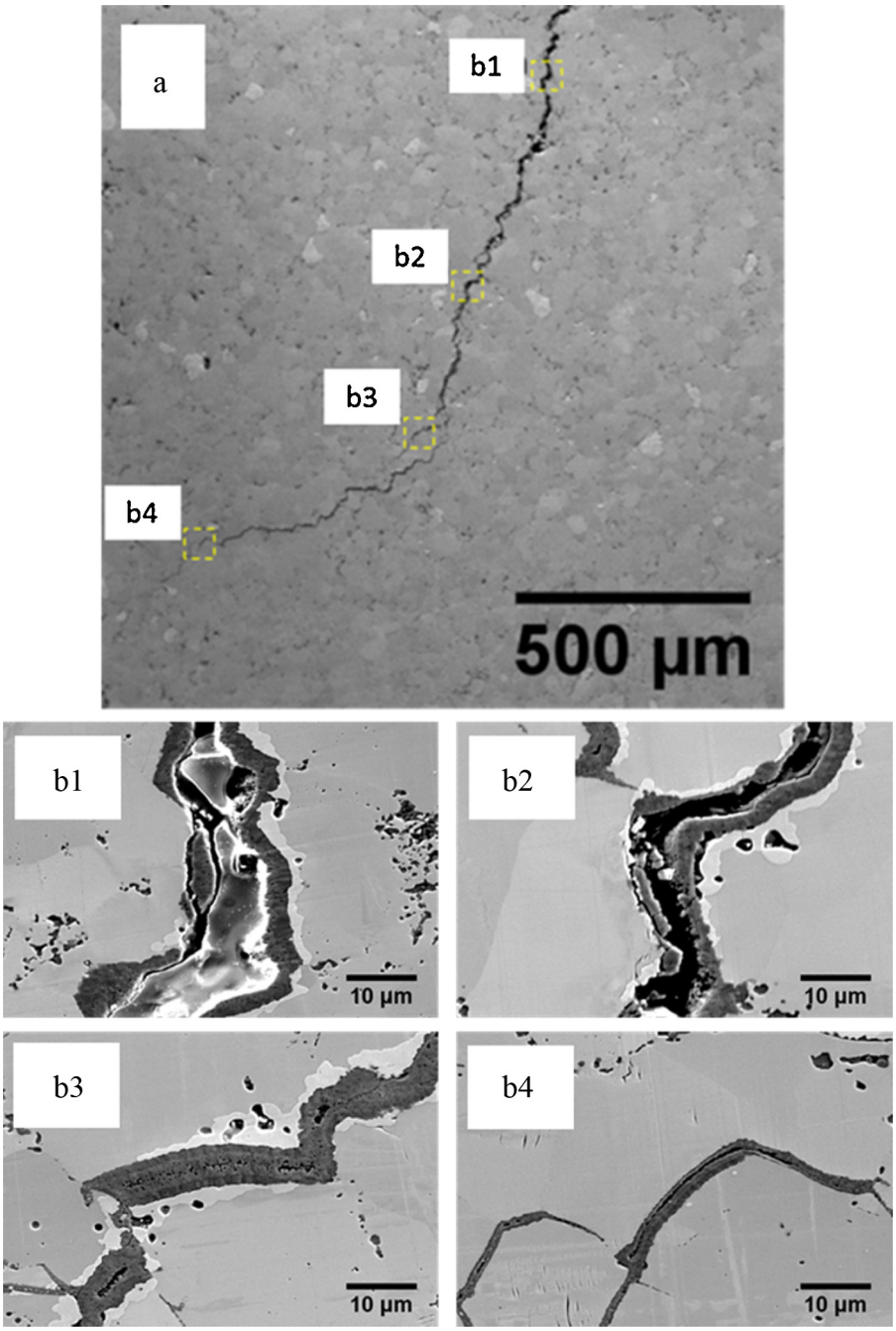

Fig. 5. Cross sectional secondary electron SEM images of a crack after healing at 1200 °C for 4 h in air: (a) a cross section image parallel to the crack growth direction of the healed crack at low magnification; (b) higher magnification images for the areas of "b1", "b2","b3","b4" in Fig. 5a.

Table 1
Average Al_2O_3 width on a single crack surface calculated along crack.

Position	b1	b2	b3	b4
Average width of Al_2O_3 (μm)	2.45	2.37	2.43	1.08

is attributed to the tolerance of Cr_2AlC to Al vacancies, maintaining the crystal structure of the matrix even when the density of Al vacancy is low. As a result, if the crack gap is small, it can be filled without the formation of Cr_7C_3 phase. However, if the crack gap is relatively wide, the depletion of Al in the nearby matrix gives rise to the Cr_2AlC structure being unstable causing it to decompose to form Cr_7C_3.

4. Discussion

4.1. Dependence of crack healing kinetics on crack location

Cracks in polycrystalline Cr_2AlC MAX phase ceramic samples usually follow the basal plane of Cr_2AlC crystals, resulting in a zigzag crack shape in non-textured Cr_2AlC samples as evident in Fig. 5a. The zigzag crack shape as well as the occurrence of crack bridging, makes it difficult to transport oxygen from the sample exterior to the root of the crack. Therefore, during the crack healing process, the oxide scale growth may happen under different local oxygen partial pressures. To investigate the potential influence of local oxygen partial pressure on overall healing rate, two

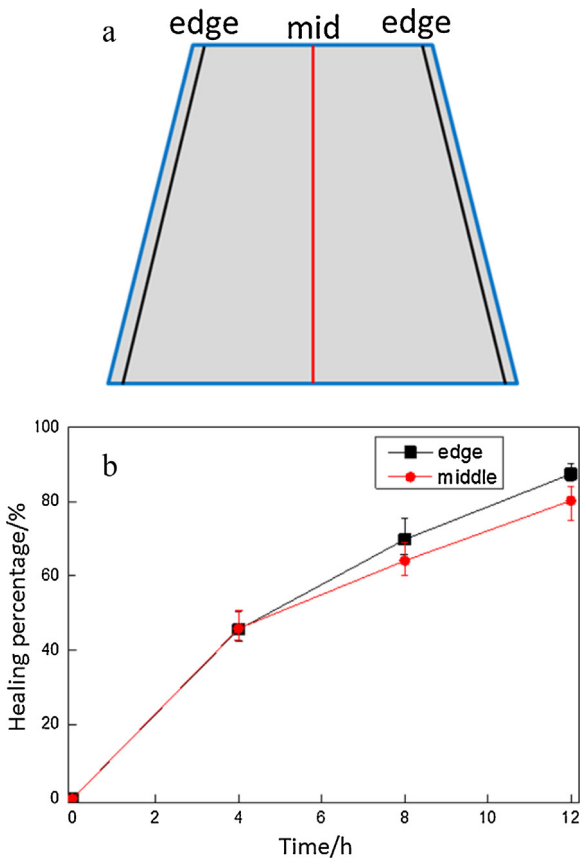

Fig. 6. (a) Lines along which the percentage healing was quantified. (b) Percentage of crack healing as a function of healing time calculated at middle and edge of the crack, respectively.

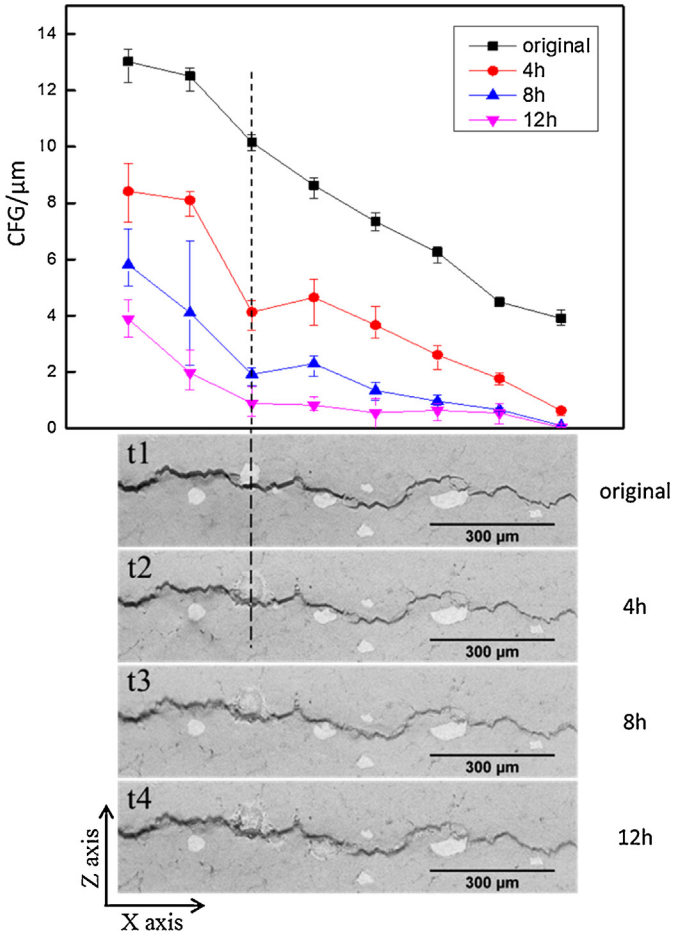

Fig. 7. (top) Crack face gap (CFG) calculated along the crack growth direction for different healing times; (below) 2D X-ray tomographic cross sections correlated to the CFG plots at different healing stages. The dashed line indicates the large CFG decrease near surface breaking Cr particle.

rather different areas of the crack are chosen. Areas very close to the crack edges are assumed to have an easier access to oxygen, thus a higher oxygen partial pressure, equal to the external oxygen partial pressure. For areas in the middle of the crack, the oxygen partial pressure could be the lower as the oxygen transport distance is longer. The overall healing percentage as a function of time at these two positions is shown in Fig. 6b.The healing percentage (percentage of the crack gap filled) as a function of time at crack middle is calculated by segmenting and measuring crack area (A(t)) in five 2D X-ray tomographic slices along the crack growth direction (along x axis), hence: $H = \frac{A(t=0)-A(t)}{A(t=0)} \times 100\%$. The healing kinetics of the crack edge was determined by averaging the healing percentages at the two crack edges.

The healing process at the edge and middle seems to show very similar trends. After the initial 4 h heat treatment, the healing percentage at the edge and middle is almost identical at about 45%. As heat treatment time increases, the healing rate in both the middle and edge decrease as one would expect given the longer diffusion distances for the Al atoms and O atoms. After 12 h healing, the percentage of the crack opening healed for the edge and middle reached about 87% and 80% respectively. This small difference suggests that for the dimensions of the current sample and its crack, the overall healing rate of Cr_2AlC is more or less independent of the oxygen partial pressure variance or that the rate of oxygen transport in the crack is sufficient to maintain a more or less constant oxygen partial pressure along the crack.

To quantify the dependence of the local healing kinetics on crack location, the crack face gap along the crack propagation direction at different healing stages is calculated and shown in Fig. 7. Each data point represents the average crack face gap (CFG) of the nearby 200 pixels (135 μm) along the crack growth direction. The initial crack was about 1000 μm in length and 13 μm wide at the crack root. After exposure in air for 4 h, despite an uncharacteristically large decrease in CFG identified by the dashed line, the CFG has reduced more or less equally at all points along the crack at round 4.5 μm. This result indicates a uniform local healing rate from crack root to crack tip. After 12 h healing, the 1000 μm long crack was healed to a new maximum length of less than 300 μm (4 μm in width at crack root). The unusually large decrease in CFG at the location indicated by the dashed line was due to the presence of Cr particles and is consistent with the observations relating to Fig. 2. The mechanism of this phenomenon will be discussed in Section 4.3.

This independence of the overall and local healing rate on crack location shown above is probably due to the fact that Cr_2AlC has a relatively slow healing kinetics when compared to many of its counterparts, such as Ti_2AlC and Ti_3AlC_2 [4,5,16,25]. The growth rate of Al_2O_3 scale is controlled by grain boundary diffusion of Al and O through existing oxide layer even at crack tip and middle, where the oxygen partial pressure is lower due to oxygen transport difficulty. The crack location induced oxygen partial pressure variance thus has a minor effect on the healing kinetics. As a result, a more or less uniform healing kinetics both along and across the crack was observed.

It is also worth noting that this uniform healing kinetics over the whole crack area means that because the crack is narrowest at the crack tip it will always heal first, while the crack root having a larger crack face gap will be fully healed last, as is indeed observed in Fig. 3.

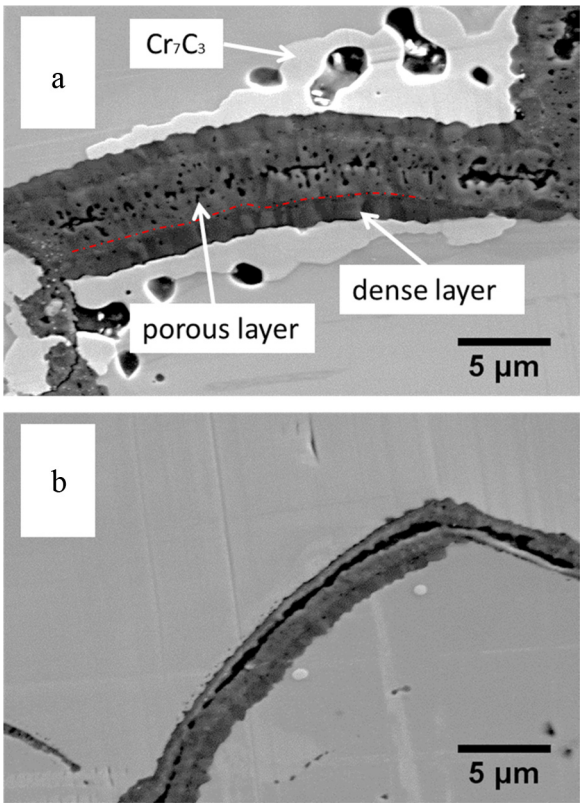

Fig. 8. High magnification secondary electron SEM images of a) region b3 and b) region b4 shown in Fig. 6. The red dashed line in (b) indicates the border between the porous and dense Al_2O_3 formed on the Cr_2AlC substrate.

In this way, the crack surface heals from crack tip to crack root. This even rate of oxide growth inhibits the propensity for blockage of the oxygen path caused by uneven local healing so that a high healing percentage can be achieved not only at crack edge but also at crack centre and crack tip (shown in Fig. 6); this is critical for good recovery of strength after healing because it reduces the likelihood of internal healing defects.

4.2. Healing mechanism of Cr_2AlC

Previous research on the oxidation of Cr_2AlC showed that the oxide grows through inward diffusion of oxygen and outward diffusion of Al [16,18–20]. In the case of crack filling, oxide growth will stop once the crack is fully filled with oxide. High magnification SEM images of the healed area at locations b3 and b4 in Fig. 5 are shown in Fig. 8. It can be seen in Fig. 8a that the oxide scale formed on the Cr_2AlC substrate after 4 h healing at 1200 °C consists of two sub-layers: an inner dense columnar Al_2O_3 layer around 1.5 μm in thickness and an outer porous Al_2O_3 layer around 1 μm in thickness. Similar oxide scale microstructures were found in the Ti_2AlC MAX phase ceramic after exposure in air at 1200 °C for 100 h [9]. For the oxide scale formed near the crack tip in Fig. 8b, only the dense columnar Al_2O_3 layer is observed. These results suggest that the porous Al_2O_3 layer was formed after the formation of the dense layer of columnar Al_2O_3.

The recovery of the strength of Cr_2AlC after healing is directly related to the microstructure and constitution of the healed region. Therefore, it is reasonable to divide the healing process into two stages: An early stage where the dense and columnar Al_2O_3 is the main oxidation product and a later stage in which a porous Al_2O_3 layer is formed on top of the dense columnar Al_2O_3 layer. In the early stage, Al is preferentially oxidized because of a more negative Gibbs formation energy of Al_2O_3 ($\Delta G_{Al2O3} << \Delta G_{Cr2O3}$). The alumina scale grows perpendicular to the Cr_2AlC substrate to form the columnar Al_2O_3, due to a higher element gradient of oxidation atoms. Once a continuous dense Al_2O_3 layer is formed, the rate of lattice diffusion of the Cr and Al atoms to the surface is significantly reduced. However, due to a relatively weak Cr—Al bond and a strong Cr—C bond, selective oxidation of Al will still occur through mass transport via the grain boundaries of the columnar Al_2O_3. At this stage, grain boundary diffusion is the dominant diffusion mechanism and a porous Al_2O_3 is formed on top of the previously formed columnar Al_2O_3 layer. The further consumption of Al results in the decomposition of Cr_2AlC matrix, giving rise to a Cr_7C_3 sublayer underneath the Al_2O_3 layer, leaving pores near the interface between Cr_7C_3 and Cr_2AlC matrix. Therefore, for short cracks with a small crack width, the crack gap is expected to be filled with dense Al_2O_3 scale, yielding good strength recovery after healing. While the recovery of strength of a long (open) crack may be less effective because of the porous Al_2O_3 layer formed in the healed region as well as the micro pores formed near the interface of Cr_7C_3 layer and Cr_2AlC matrix. In addition micro cracks were observed at the interface of Al_2O_3 layer and Cr_7C_3 layer, as shown in Fig. 5b2. This is probably due to the buildup of thermal stress during cooling by the differences of thermal expansion coefficient between Al_2O_3 ($8 \times 10^{-6}\,K^{-1}$) and Cr_7C_3 ($10.6 \times 10^{-6}\,K^{-1}$ [18]). The existence of these interfacial cracks could be detrimental for strength recovery.

The crack healing kinetics can be assessed in terms of the evolution in the gap between the crack faces (CFG) during healing plotted in Fig. 9a. Unlike TGA experiments, which are usually performed on a polished surface [16,18], the CFG measurement represents the oxide growth over a serrated crack surface. The results show a decrease in healing rate with time broadly consistent with parabolic (diffusion controlled) growth. The oxide scale thickness curve fitting result (h is the oxide scale thickness on a single crack surface) shows that the kinetics of healed crack width broadly follows a parabolic law with a parabolic rate constant $k_p = 4.6 \times 10^{-4}\,\mu m^2\,s^{-1}$. The TGA experiment in Fig. 9c was conducted using the same batch of Cr_2AlC material under the same oxidation condition. Compared with the oxide growth over a flat surface (as obtained from TGA, shown in Fig. 9c), the oxide growth over a serrated crack surface is significantly faster. The higher nucleation density at a serrated surface and thus smaller grain size of the oxide may be responsible for this faster growth, which is beneficial for the crack healing. A similar phenomenon was observed in the healing of a cavity on a Ti_2AlC matrix [9], where the grain size of formed Al_2O_3 is smaller than that on a flat surface, indicating a faster nucleation density.

4.3. The effect of chromium particles

The results in Figs. 2 and 7 indicate that the presence of Cr particles may locally accelerate the healing process of nearby crack surfaces. This phenomenon is very interesting, because the presence of local Cr-rich residues could be turned into a positive factor for the healing ability. Due to their presence, the intrinsic self-healing Cr_2AlC material is effectively turned into a mixed intrinsic-extrinsic self-healing material. To further investigate this phenomenon, a correlative analysis was conducted on the Cr_2AlC sample which had been previously tracked by time-lapse X-ray tomography. The sample was ground away layer-by-layer in the crack direction until the region of interest identified by tomography was reached (see Fig. 10).

The secondary electron SEM image (Fig. 10e) matches well with the X-ray tomographic slices (Fig. 10d). It can be seen in the virtual tomographic sections Fig. 10a-d that two Cr particles (particle 1 and particle 2) lie in close proximity to the fracture surface, as indicated by arrows in Fig. 10a. The original crack passed through

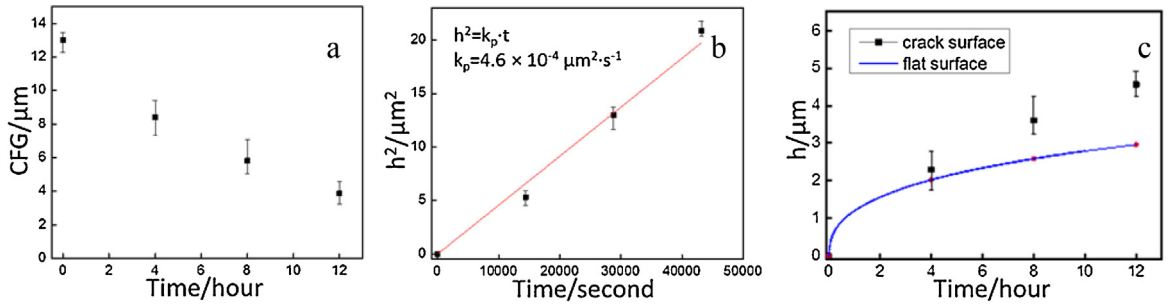

Fig. 9. (a) Crack face gap at crack root as a function of healing time determined from five 2D virtual X-ray CT slices. (b) Square of the healed crack width (h) as a function of healing time. (c) Oxide scale thickness as a function of time on serrated crack surface and flat surface. The TGA experiment was conducted using the same batch of Cr_2AlC material under the same oxidation condition, i.e. at 1200 °C in air.

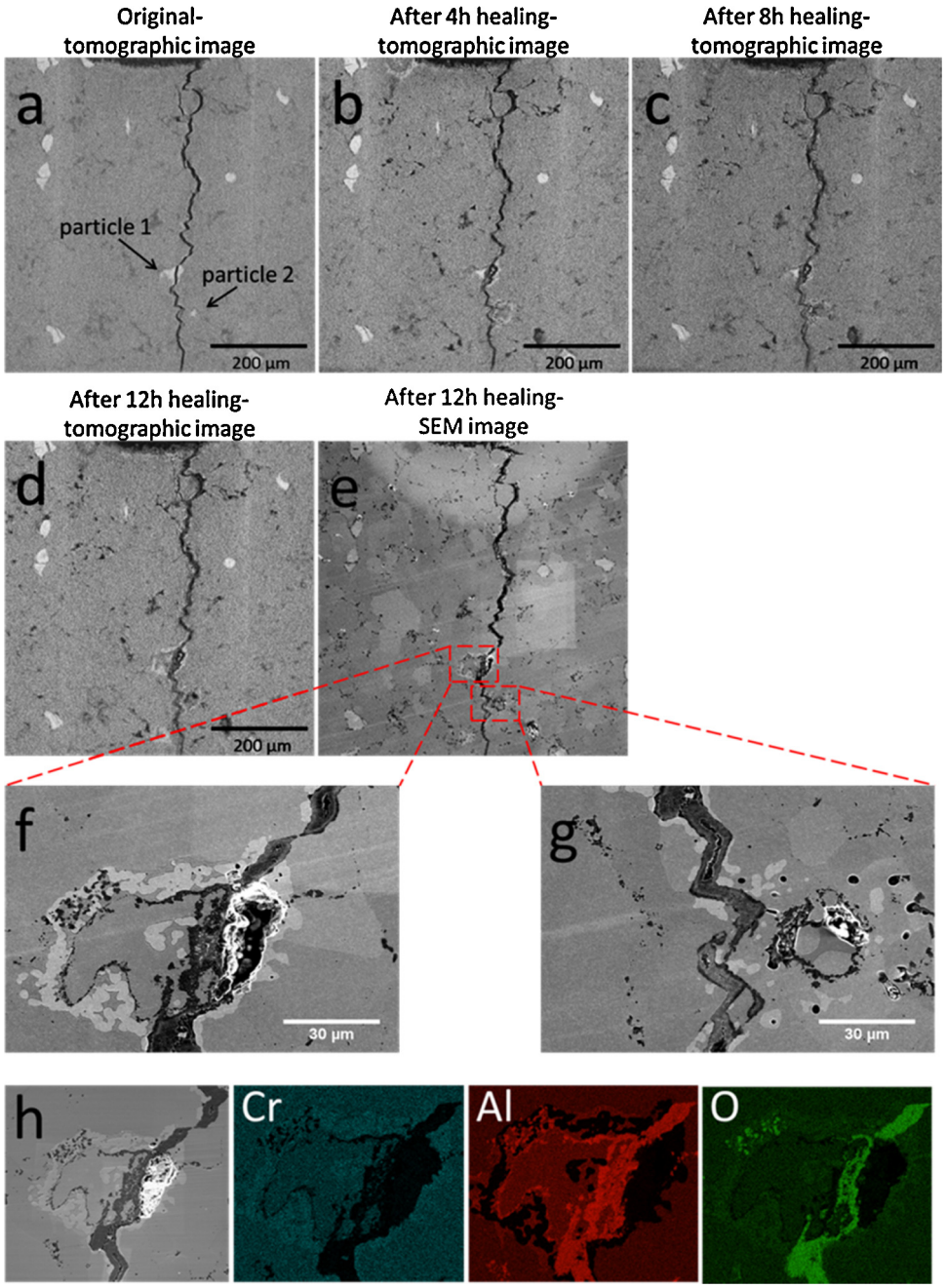

Fig. 10. (a–d) Time lapse sequence of virtual X-ray tomographic slices of the same region-of-interest as a function of healing time (crack grew from top to bottom) at 1200 °C in air. (e) Secondary electron SEM cross section of the same region-of-interest correlated to (d). (f-g) Higher magnification SEM images of the healed regions indicated by the red rectangles in (e). (h) EDS elemental maps of the region in (f). Particle 2 lies predominantly below the current virtual slice.

particle 1, breaking it into two smaller parts. Although it seems that the particle 2 was not in direct contact with the crack, in successive tomographic slices beneath the current slice, the crack propagated along the interface of Cr particle 2 and the Cr_2AlC matrix (not shown here for brevity). After 4 h of annealing at 1200 °C, the right half of particle 1 has been consumed, leaving a white layer around the original shape of the Cr particle, as shown in Fig. 10b. In the meantime, the larger left half of particle 1 also shrunk and was completely consumed after 12 h of heat treatment at 1200 °C, as shown in Fig. 10d. A similar white layer is observed around the original position of the left half of particle 1. A higher magnification SEM image of the healed area near the Cr particle and the corresponding elemental mappings are shown in Fig. 10f and 10 h. Consistent with the virtual tomographic slices, a grey area (composed of Cr and Al) is observed surrounded by white layers (composed of Cr and C), shown in Fig. 10f. A similar interaction is observed between the crack and particle 2. However, in this case the Cr_7C_3 layer gradually disappeared with prolonged healing. After 12 h of heat treatment the Cr_7C_3 was consumed leaving a pore, as shown in Fig. 10g.

Based on the above observations, it is proposed that initially the atmospheric oxygen partial pressure is high enough for the exposed Cr particles to oxidize to Cr_2O_3. The existence of surface breaking Cr particles during healing results in the formation of Cr_2O_3 particles or films provides a nucleation site of Al_2O_3, thus increasing the rate of formation of Al_2O_3. The relatively rapid consumption of Al atoms creates a large chemical potential for Al to diffuse from nearby Cr_2AlC matrix to the crack surface. In order to diffuse from the Cr_2AlC matrix to the crack surface, the Al atoms has to pass through the Cr particles, resulting into the enrichment of Al in Cr particles. Element ratio calculations from EDS suggest that the surface breaking Cr particles changed to a chemical composition of Cr:Al = 1:1. However, it should be aware that such compound does not exist in the Cr-Al phase diagram and a more detailed study is needed to fully understand this interesting phenomenon.

A further depletion of Al at the Cr-Cr_2AlC interface makes the nearby Cr_2AlC matrix become unstable and this results in the formation of a Cr_7C_3 layer. At longer healing times, Cr_7C_3 reacts with oxygen to form Cr_2O_3, which is transformed to the gaseous CrO_3 phase at the imposed high temperature [26,27]. The vaporization of CrO_3 leaves pores in the healed area, which may have a negative effect on strength recovery after healing.

5. Conclusions

Our results have demonstrated that non-destructive time-lapse X-ray tomographic imaging together with post-mortem correlative SEM can be used to track the crack healing process of Cr_2AlC in great detail. Healing of a crack in Cr_2AlC at 1200 °C in air is followed as a function of the annealing time in 3D with a pixel size of 0.68 μm, providing data to develop and validate crack healing models of this material. Based on our current results, the following conclusions could be reached:

I. The crack healing of Cr_2AlC is an oxidation process where the crack gap is filled essentially by Al_2O_3. The maximum crack width that could be fully healed at 1200 °C in air within 4 and 12 h is estimated to be around 4.8 μm and 10 μm respectively.
II. During healing Cr_7C_3 phase is observed when the crack width exceeds 2 μm.
III. The Al_2O_3 scale comprises a porous layer on top of a columnar dense layer typically 1.5 μm thick after 4 h' healing at 1200 °C. The former is not observed for the repair of the crack when it is less than 2 μm wide.
IV. Despite the two layer nature of the repair, the crack healing kinetics of Cr_2AlC at 1200 °C in air broadly follows a parabolic rate law with constant of 4.6×10^{-4} μm^2 s^{-1}.
V. The existence of impurity Cr particles locally accelerated the healing process by providing Cr_2O_3 nucleation sites. The later evaporation of Cr_2O_3 may leave large pores near the healed area, which may reduce strength recovery.

Acknowledgements

The authors would like to thank China Scholarship Council for providing the financial support for this research. The Henry Moseley X-ray Imaging Facility, University of Manchester, was funded in part by the EPSRC (grants EP/F007906/1, EP/F001452/1 and EP/I02249X/1).We also acknowledge the financial support by the German Research Foundation (Deutsche Forschungsgemeinschaft, DFG, SPP 1568'Design and Generic Principles of Self-Healing Materials', under contract SL184/1-2).

References

[1] M.W. Barsoum, M. Radovic, Elastic and mechanical properties of the MAX phases, Annu. Rev. Mater. Res. 41 (2011) 195–227.
[2] M. Radovic, M.W. Barsoum, MAX phases: bridging the gap between metals and ceramics, Am. Ceram. Soc. Bull. 92 (3) (2013) 20–27.
[3] Y. Zhou, X. Wang, Deformation of polycrystalline Ti_2AlC under compression, Mater. Res. Innovations 5 (2) (2001) 87–93.
[4] X. Wang, Y. Zhou, Oxidation behavior of Ti_3AlC_2 at 1000–1400 °C in air, Corros. Sci. 45 (5) (2003) 891–907.
[5] X. Wang, Y. Zhou, High-temperature oxidation behavior of Ti_2AlC in air, Oxid. Met. 59 (3–4) (2003) 303–320.
[6] G.P. Bei, G. Laplanche, V. Gauthier-Brunet, J. Bonneville, S. Dubois, Compressive behavior of Ti_3AlC_2 and $Ti_3Al_{0.8}Sn_{0.2}C_2$ MAX phases at room temperature, J. Am. Ceram. Soc. 96 (2) (2013) 567–576.
[7] M.W. Barsoum, T. El-Raghy, The MAX phases: unique new carbide and nitride materials-ternary ceramics turn out to be surprisingly soft and machinable, yet also heat-tolerant, strong and lightweight, Am. Scientist 89 (4) (2001) 334–343.
[8] W. Tian, Z. Sun, H. Hashimoto, Y. Du, Compressive deformation behavior of ternary compound Cr_2AlC, J. Mater. Sci. 44 (1) (2009) 102–107.
[9] H. Yang, Y. Pei, J. Rao, J.T.M. De Hosson, S. Li, G. Song, High temperature healing of Ti_2AlC: on the origin of inhomogeneous oxide scale, Scr. Mater. 65 (2) (2011) 135–138.
[10] H. Yang, Y. Pei, J.T.M. De Hosson, Oxide-scale growth on Cr_2AlC ceramic and its consequence for self-healing, Scr. Mater. 69 (2) (2013) 203–206.
[11] S. Li, G. Song, K. Kwakernaak, S. van der Zwaag, W.G. Sloof, Multiple crack healing of a Ti_2AlC ceramic, J. Eur. Ceram. Soc. 32 (8) (2012) 1813–1820.
[12] A.S. Farle, C. Kwakernaak, S. van der Zwaag, W.G. Sloof, A conceptual study into the potential of $M_{n+1}AX_n$-phase ceramics for self-healing of crack damage, J. Eur. Ceram. Soc. 35 (1) (2015) 37–45.
[13] G. Song, Y. Pei, W.G. Sloof, S. Li, J.T.M. De Hosson, S. Van der Zwaag, Oxidation-induced crack healing in Ti_3AlC_2 ceramics, Scr. Mater. 58 (1) (2008) 13–16.
[14] H. Yang, Y. Pei, J. Rao, J.T.M. De Hosson, Self-healing performance of Ti_2AlC ceramic, J. Mater. Chem. 22 (17) (2012) 8304–8313.
[15] W.G. Sloof, R. Pei, S.A. McDonald, J.L. Fife, L. Shen, L. Boatemaa, A.S. Farle, K. Yan, X. Zhang, S. van der Zwaag, P.D. Lee, P.J. Withers, Repeated crack healing in MAX-phase ceramics revealed by 4D in situ synchrotron X-ray tomographic microscopy, Sci. Rep. 6 (2016).
[16] W. Tian, P. Wang, Y. Kan, G. Zhang, Oxidation behavior of Cr_2AlC ceramics at 1 100 and 1250 °C, J. Mater. Sci. 43 (8) (2008) 2785–2791.
[17] D.J. Tallman, B. Anasori, M.W. Barsoum, A critical review of the oxidation of Ti_2AlC, Ti_3AlC_2 and Cr_2AlC in air, Mater. Res.Lett. 1 (3) (2013) 115–125.
[18] D. Lee, S. Park, Oxidation of Cr_2AlC between 900 and 1200 °C in air, Oxid. Met. 68 (5–6) (2007) 211–222.
[19] D.B. Lee, T.D. Nguyen, S.W. Park, Long-time oxidation of Cr_2AlC between 700 and 1000 °C in air, Oxid. Met. 77 (5–6) (2012) 275–287.
[20] S. Li, L. Xiao, G. Song, X. Wu, W.G. Sloof, S. van der Zwaag, Oxidation and crack healing behavior of a fine-grained Cr_2AlC ceramic, J. Am. Ceram. Soc. 96 (3) (2013) 892–899.
[21] Z. Lin, Y. Zhou, M. Li, J. Wang, In-situ hot pressing/solid-liquid reaction synthesis of bulk Cr_2AlC, Z. Metallkunde 96 (3) (2005) 291–296.
[22] X. Duan, L. Shen, D. Jia, Y. Zhou, S. van der Zwaag, W.G. Sloof, Synthesis of high-purity, isotropic or textured Cr_2AlC bulk ceramics by spark plasma

sintering of pressure-less sintered powders, J. Eur. Ceram. Soc. 35 (5) (2015) 1393–1400.
[23] E. Maire, P.J. Withers, Quantitative X-ray tomography, Int. Mater. Rev. 59 (1) (2014) 1–43.
[24] W. Tian, P. Wang, Y. Kan, G. Zhang, Oxidation behavior of Cr_2AlC ceramics at 1 100 and 1,250 °C, J. Mater. Sci. 43 (8) (2008) 2785–2791.
[25] X. Wang, Y. Zhou, Oxidation behavior of Ti_3AlC_2 powders in flowing air, J. Mater. Chem. 12 (9) (2002) 2781–2785.
[26] R. Grimley, R. Burns, M.G. Inghram, Thermodynamics of the vaporization of Cr_2O_3: dissociation energies of CrO, CrO_2, and CrO_3, J. Chem. Phys. 34 (2) (1961) 664–667.
[27] M. Stanislowski, E. Wessel, K. Hilpert, T. Markus, L. Singheiser, Chromium vaporization from high-temperature alloys I. Chromia-forming steels and the influence of outer oxide layers, J. Electrochem. Soc. 154 (4) (2007) A295–A306.